Sensitivity of G_0 and stress-strain relation of geomaterials to grain shape and surface roughness

Masahide Otsubo[1,2#], *Yang* Li[2], and *Reiko* Kuwano[2]

[1]*Public Works Research Institute, 1-6 Minamihara, Tsukuba, Ibaraki 305-8516, Japan*
[2]*The University of Tokyo, Institute of Industrial Science, 4-6-1 Komaba, Meguro-ku, Tokyo 153-8505, Japan*
[#]*Corresponding author: ootsubo-m573cm@pwri.go.jp*

ABSTRACT

It is empirically known that the packing property and mechanical responses of cohesionless granular materials are influenced by grain shape. For example, the attainable range of void ratio depends on grain shape; angular materials tend to exhibit greater friction angles. Besides, shear wave velocity (V_s) and small-strain shear modulus (G_0) of sphere assemblies are affected by surface roughness. However, consensus has yet to be reached on the combined effect of grain shape and surface roughness on G_0 and stress-strain relation. This contribution aims to evaluate the shape-roughness combined effect on the strain-dependent mechanical responses of granular materials. Three groups of glass beads having different grain shapes and a silica sand were used, and their grain surfaces were roughened through a systematic procedure using a milling machine. In total, eight materials were subjected to triaxial compression after measurement of V_s. The experimental results reveal that the stress-strain relation of angular particles is remarkably affected by the surface roughness, whereas the roughness effect on the stress-dependent variation in G_0 is limited for angular particles.

Keywords: Grain shape; surface roughness; stiffness; strength.

1. Introduction

Granular materials are composed of a large number of particles and their overall mechanical response can be considered as a consequence of complicated interactions of grains. It is empirically known that both packing characteristics and stress-strain relation of cohesionless granular materials are influenced by grain shape (Cho et al. 2006; Altuhafi et al. 2016). It has also been demonstrated that shear wave velocity (V_s) and thus small-strain shear modulus (G_0) of sphere assemblies tend to be lower for spherical particles having rougher surfaces (Santamarina and Cascante 1998; Sharifipour and Dano 2006; Otsubo et al. 2015). However, consensus has yet to be reached on the potential effect of surface roughness on friction angles. Further, there has been little consideration on the combined effect of grain shape and surface roughness on the G_0 and stress-strain relation.

This contribution aims to evaluate the shape-roughness combined effect on the strain-dependent mechanical responses of granular materials focusing on both stiffness and strengh characteristics in experiments.

Table 1. Particle properties (G_s: specific gravity) and shape parameters (S: sphericity; C_x: convexity; AR: aspect ratio, Altuhafi et al. 2013)

ID	G_s	D_{50} [mm]	C_u	S	C_x	AR
SSGB	2.50	0.496	1.15	0.940	0.974	0.975
SDGB	2.50	1.040	1.17	0.844	0.982	0.784
SAGB	2.50	0.746	1.31	0.786	0.959	0.631
NSS	2.64	0.525	1.46	0.857	0.936	0.720

2. Materials

Three groups of glass beads (GB) with different grain shapes and a silica sand (SS), having low unifornity coefficients (C_u), were used (Table 1). The three glass beads are spherical (SGB), deformed (DGB) and angular (AGB). Their as-supplied surfaces were roughened using a milling machine (Fig. 1) following Dutta et al. (2020). Each material and a fine silica sand (D_{50}=0.15 mm) were mixed in a ceramic jar having a ratio of 1:2 by mass, and rotated for 48 hours with about 1.5 Hz. The as-supplied natural silica sand (NSS) was also roughened to prepare rough-surface silica sand (RSS). Grain sizes and shapes of the as-suplied materials were measured using a QICPIC apparatus (Altuhafi et al. 2013), and they were asuumed unchanged through the gentle milling process. The extream void ratios (e_{min} and e_{max}) for the tested materials are given in Table 2. The average and root-mean suqre surface roughness (S_a and S_q) were quantified using Gaussian filter method (Li et al. 2021).

Table 2. Surface roughness and extreme void ratios

ID	S_a [nm]	S_q [nm]	e_{min}	e_{max}
SSGB	38.9	67.6	0.589	0.694
RSGB	114.3	173.5	0.606	0.696
SDGB	97.5	154.8	0.494	0.666
RDGB	171.7	232.0	0.509	0.683
SAGB	75.0	127.2	0.734	1.176
RAGB	148.0	224.7	0.745	1.170
NSS	424.3	680.0	0.719	1.122
RSS	479.9	795.4	0.716	1.060

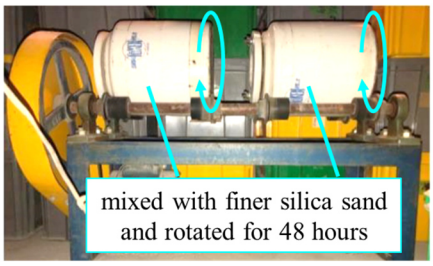

Figure 1. Milling machine used to roughen grain surface.

3. Test method

The adopted test method in this contribution is described in detail in Li (2022) that broadly follows the approach in Dutta et al. (2020; 2021).

3.1. Sample preparation

Cylindrical samples having 75 mm in diameter and 150 mm in height (H) were prepared using a split mould. Dry materials were carefully poured in air using a funnel and gentle side tapping was given to the mould to densify the sample to vary initial void ratio (e) and relative density (D_r) in a systematic manner. Each material was prepared at least two distinct density levels.

Samples were then subjected to an initial isotropic stress (p_0') of 50 kPa under dry and drained conditions by applying negative pressure, where V_s was measured as explained in the following section. For the stress levels above 50 kPa, cell pressure was applied to the sample under dry and drained conditions. One axial displacement sensor (linear variable differential transducer, LVDT) and three radial displacement transducers (clip gauges, CGs) were placed to monitor the deformation of the sample under dry and drained conditions (Fig. 2).

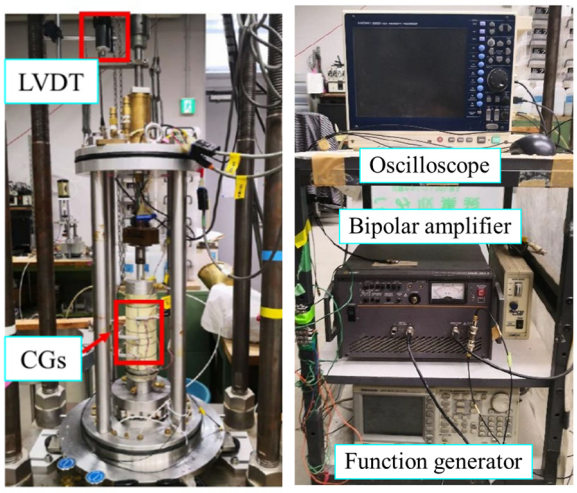

Figure 2. Test equipment used: (left) triaxial apparatus, (right) shear wave measurement system.

3.2. Shear wave measurement

At the initial isotropic state of 50 kPa, shear wave measurement was conducted using shear plates (Fig. 3). The system comprises of shear (S-) and compression (P-) type piezoelectric plates, having 20 mm in diameter and 2 mm in thickness, inside a hollow stainless-steel cylinder, which is supported by epoxy glue and silicone (Fig. 3) as presented in Dutta et al. (2021). This contribution utilizes the S-wave data (from shear-type plate) to determine shear wave velocity (V_s) measured in the vertical direction.

Two conventional methods for estimating the travel time from time-domain responses are peak-to-peak (ptp) and start-to-start (sts) methods. Yamashita et al. (2009) recommend that input frequency (f_{in}) should be selected such that ptp and sts methods give comparable V_s. Following Dutta et al. (2020; 2021), this contribution uses a single-period sinusoidal form having f_{in} of 7 kHz as an inserted wave. The travel time (T_T) of shear waves was determined using the ptp method. Typical wave signals measured for the tested materials are presented in Li (2022). To amplify the received signals, the inserted voltage was amplified to ±70 V via a bipolar amplifier (Fig. 2). V_s was calculated as H/T_T.

Assuming an isotropic and homogeneous condition, the following relation can be used to estimate G_0 from V_s measured in the vertical direction.

$$G_0 = \rho_d V_s^2 \tag{1}$$

where ρ_d is the dry density of the sample and is expressed as $G_s\,\rho_w/(1+e)$; ρ_w is the density of water.

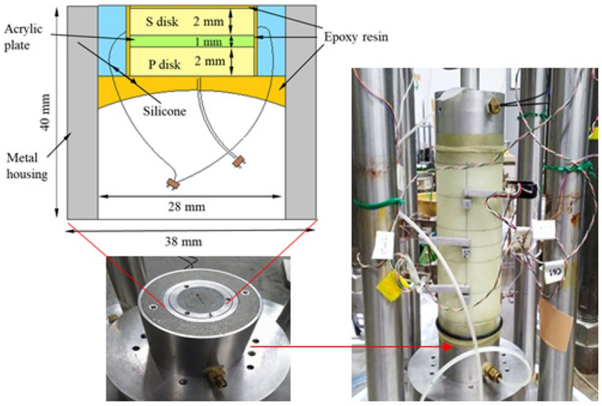

Figure 3. Schematic of shear plates (disk-shaped transducers) in metal housing inside top cap and pedestal (Dutta et al. 2021).

3.3. Triaxial compression

After conducting shear wave measurement at p_0' = 50 kPa, the sample was monotonically sheared by increasing the axial strain up to ε_a of about 15% (defined as the residual state in this study). The minor principal stress (σ_3') was kept at 50 kPa while increasing the axial stress (σ_1'). A constant strain rate of 0.0006 %/s was adopted to record shear wave signals at target axial strains. During the shearing, deviator stress, $q = \sigma_1' - \sigma_3'$, and mean effective stress, $p' = (\sigma_1' + 2\sigma_3')/3$ were recorded. In the following section, the evolution of deviator stress ratio (q/p') against ε_a is discussed. Besides, mobilized peak and residual friction angles (φ_{peak} and φ_{res}) for each material are provided. While the data are not presented here, Li (2022) reports the evolutions of volumetric strain and S-and P-wave velocities during the shearing process.

4. Stress-strain relation

4.1. Spherical glass beads (SGB)

For smooth-surface and rough-surface spherical glass beads (SSGB and RSGB, Fig. 4), stress-strain curves for three samples having different initial e are plotted in Fig. 5. Regarding the peak strength, RSGB samples having a rough surface exhibit slightly greater φ_{peak} values under the equivalent D_r where e is slightly higher for RSGB. Dutta et al. (2020) reported that under an equivalent e, rougher materials exhibit larger φ_{peak} than the smooth equivalent; this agrees with the result in Fig. 5. More dilation is evident for rougher materials (Li 2022). The φ_{res} values are similar between SSGB and RSGB; this trend agrees with the finding in Cavarretta et al. (2010). SSGB with higher e exhibit fluctuation in q/p'; when this is significant, φ values were calculated considering the median value of the fluctuation amplitude.

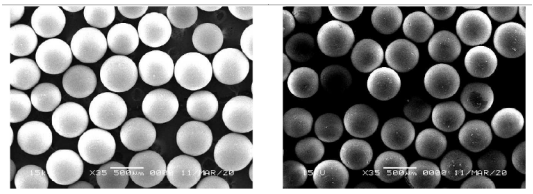

SSGB RSGB

Figure 4. SEM images of spherical glass beads having smooth surface (SSGB) and roughened surface (RSGB).

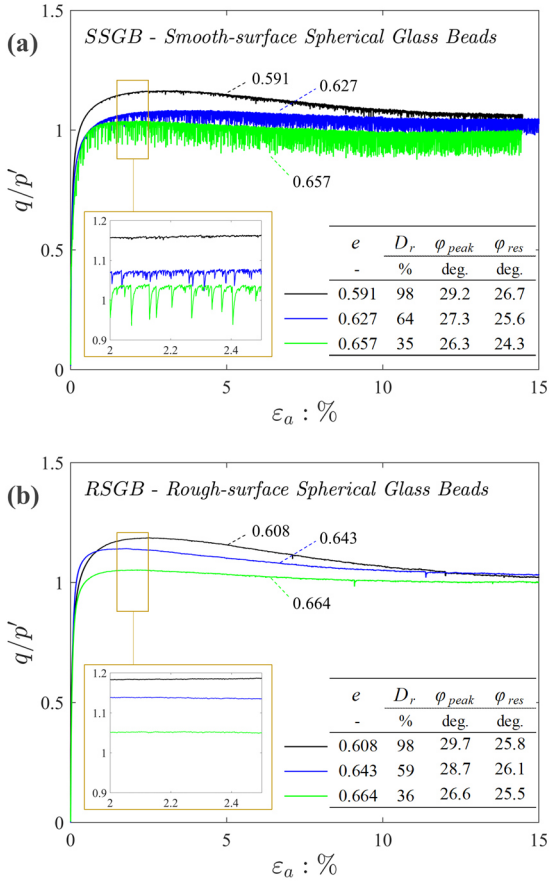

Figure 5. Stress-strain curves for (a) smooth-surface spherical glass beads (SSGB) and (b) rough-surface spherical glass beads (RSGB) at σ_3'= 50 kPa.

4.2. Deformed glass beads (DGB)

Smooth-surface deformed glass beads (SDGB, Fig. 6) were produced in the same process as SSGB, where particles having slightly deformed shapes were collected as SDGB in the manufacturing company.

Fig. 7 shows that q/p' for SDGB is clearly greater than that for SSGB or RSGB, indicating a greater contribution of grain shape than surface roughness. The effect of surface roughness appears in a similar manner with the comparison between SSGB and RSGB (Fig .5). That is, the φ_{peak} values of RDGB are slightly greater than SDGB, whereas the φ_{res} values are similar irrespective of the magnitude of surface roughness.

For the loose SDGB sample (Fig. 7a), fluctuation in q/p' is more significant than SSGB (Fig. 5a), probably due to the larger grain sizes in SDGB (Table 1). Nevertheless, the fluctuation is removed in RDGB, probably due to the prevention of inter-particle slip.

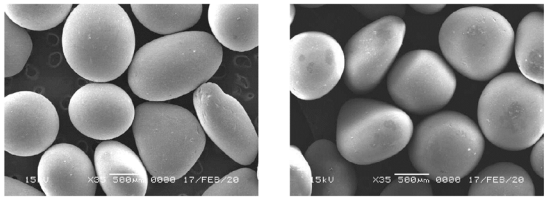

SDGB RDGB

Figure 6. SEM images of deformed glass beads having smooth surface (SDGB) and roughened surface (RDGB).

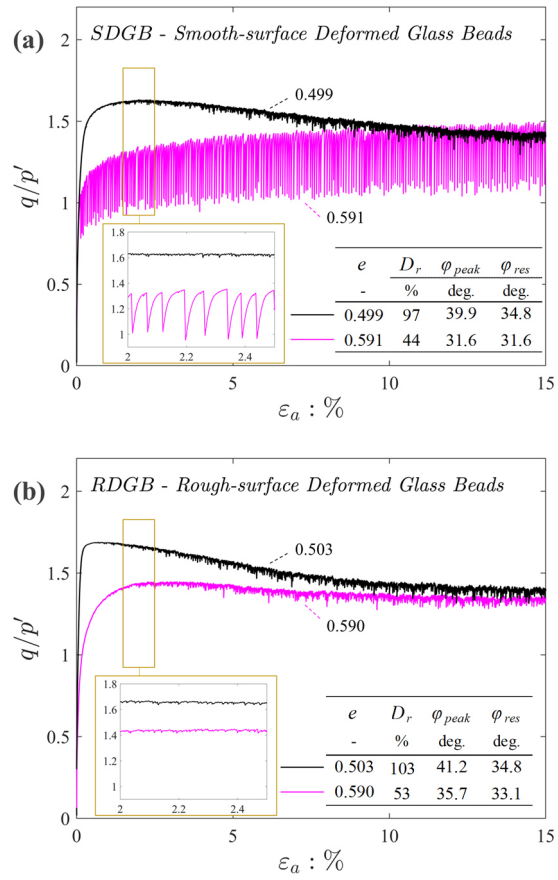

Figure 7. Stress-strain curves for (a) smooth-surface deformed glass beads (SDGB) and (b) rough-surface deformed glass beads (RDGB) at σ_3'= 50 kPa.

4.3. Angular glass beads (AGB)

Smooth-surface angular glass beads (SAGB, Fig. 8) were produced by crushing spherical glass beads in the manufacturing company. Thus, SAGB and SSGB have the same physical properties except for their grain shapes.

Fig. 9 illustrates that the φ_{peak} and φ_{res} values of AGB samples are much greater than the SGB and DGB materials despite higher e in the AGB samples. This highlights a remarkable role of grain shape. However, the initial slope of the $q/p' - \varepsilon_a$ relation of AGB samples appears lower than that for SGB and DGB samples, probably due to the difference in e or grain shape.

Contrary to SGB and DGB samples, the effect of surface roughness on AGB samples is obvious. For a similar e or D_r, both the φ_{peak} and φ_{res} values are larger for RAGB, suggesting that the effect of surface roughness is more remarkable for angular materials.

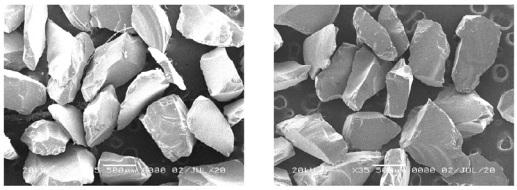

SAGB RAGB

Figure 8. SEM images of angular glass beads having smooth surface (SAGB) and roughened surface (RAGB).

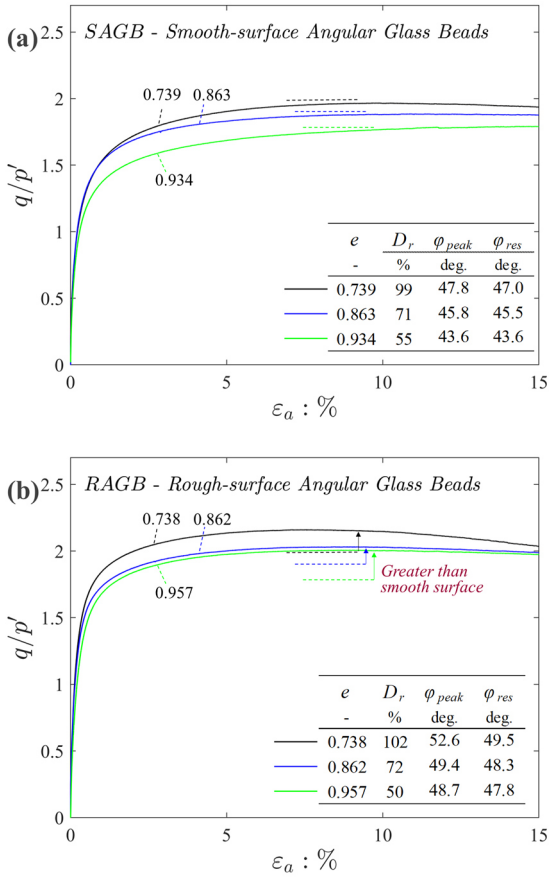

Figure 9. Stress-strain curves for (a) smooth-surface angular glass beads (SAGB) and (b) rough-surface angular glass beads (RAGB) at σ_3'= 50 kPa. Dashed lines indicate the difference between SAGB and RAGB samples at equivalent densities.

4.4. Silica sand (SS)

The natural-surface silica sand selected has been widely used in soil mechanics research in Japan. The main component is SiO_2, similar with quartz sand. In the manufacturing process, the silica sand was produced by crushing a larger mass. This process is similar with the SAGB material, and thus their shapes are indeed similar (Figs. 8 and 10). It is noteworthy that the e_{min} and e_{max} also similar between the two materials (Table 2). The natural-surface was made rougher in the same milling process adopted for RSGB, RDGB and RAGB.

The overall stress-strain curves of NSS and RSS are similar with SAGB and RAGB, respectively, where the φ_{peak} of SS samples are slightly lower than AGB samples. Under the equivalent e, the effect of surface roughness is evident; RSS exhibits greater φ_{peak} and φ_{res} values than NSS (Fig. 11).

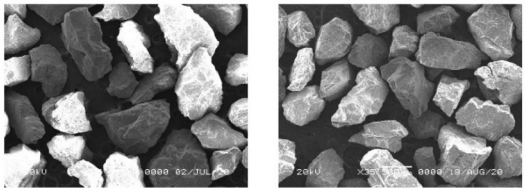

NSS RSS

Figure 10. SEM images of silica sands having natural (as-provided) surface (NSS) and roughened surface (RSS).

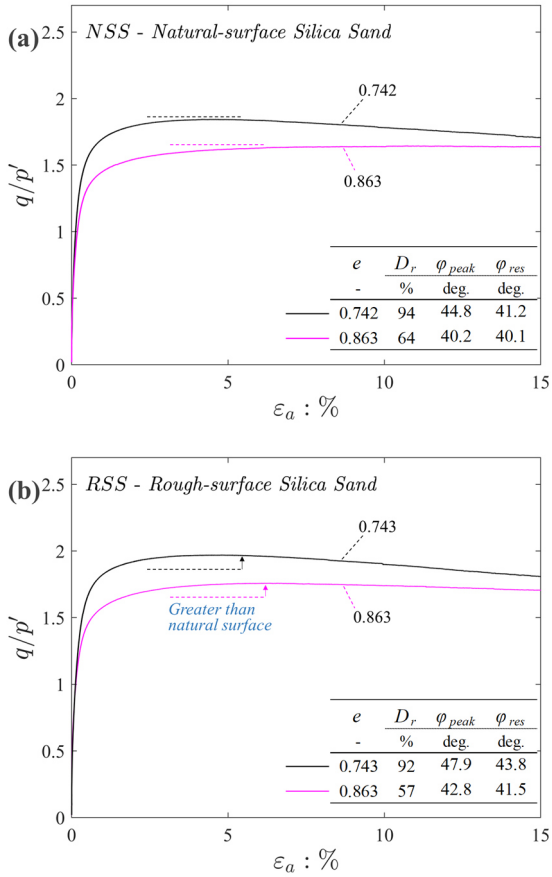

Figure 11. Stress-strain curves for (a) natural-surface (as-provided) silica sand (NSS) and (b) rough-surface silica sand (RSS) at σ_3'= 50 kPa. Dashed lines highlight the difference between NSS and RSS samples at equivalent densities.

5. Small-strain shear modulus

At p_0'= 50 kPa, V_s was measured at various e for the eight materials (Fig. 12). Referring to Table 2, each material has different e_{min} and e_{max}; SGB and DGB cannot attain e > 0.7, while AGB and SS cannot achieve e < 0.7. Fig. 12 shows fitting lines based on regression analyses for two groups separately, namely *spherical shape* (SGB and DGB) and *angular shape* (AGB and SS).

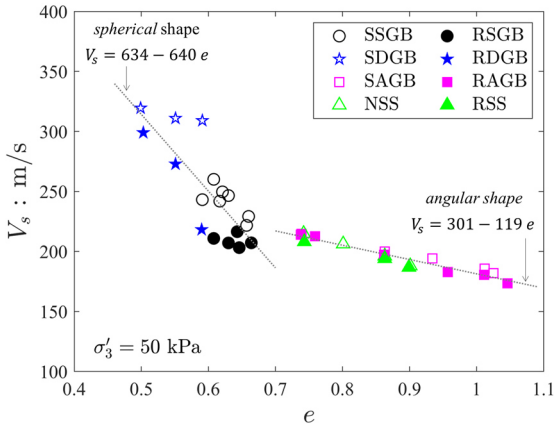

Figure 12. Relationship between V_s and e at σ_3'= 50 kPa (Fitting lines are plotted for *spherical shape* (SGB and DGB) and *angular shape* (AGB and SS), separately).

Referring to Hardin and Richart (1963), the $V_s - e$ relation can be expressed linearly as:

$$V_s = A_1 - A_2 e \tag{2}$$

$$B = A_1/A_2 \tag{3}$$

Following the approach in Hardin and Richart (1963), the B value in Eq. (3) can be used in a void ratio correction function for G_0 as:

$$f(e) = (B - e)^2/(1 + e) \tag{4}$$

The B value for SSGB alone is 1.26, similar to 1.28 for borosilicate beads (Otsubo et al. 2018) and 1.44 for the same glass bead material having a larger size (Dutta et al. 2020). However, the dataset is scattered in Fig. 12, especially for the DGB samples. Therefore, two separate fitting lines including SGB and DGB (i.e. *spherical shape*) and including AGB and SS (i.e. *angular shape*) were adopted for the later discussion, giving B = 0.991 and 2.52, respectively. The B value for the group of *angular shape* is similar to 2.97 proposed for angular grains (dry crushed quartz sands) in Hardin and Richart (1963). The overall trend in Fig. 12 also captures the transition observed between round grains and angular grains in Hardin and Richart (1963).

From Eq. (1), G_0 can be calculated as a function of e and V_s. For each material, one sample was tested at p_0'= 25, 50, 100, 200 and 400 kPa to explore the stress dependent variation of G_0 (Fig. 13). To remove the effect of void ratio on G_0 at different stress levels, Eq. (4) can be used. To express the stress-dependent evolution of G_0, the following expression is often used.

$$G_0 = \alpha\, f(e)\, {p_0'}^{\beta} \tag{5}$$

where α is the material constant and β is the stress exponent. Fig. 13 compares the evolution of G_0 for a reference void ratio of 0.6 and 0.85, respectively, for *spherical shape* and *angular shape* groups.

The magnitude of α depends on $f(e)$, and thus α depends on B. Referring to Fig. 12 and Eq. (3), this contribution uses two different B values for *spherical shape* (SGB and DGB) and *angular shape* (AGB and SS); thus, comparison on α alone is not very meaningful.

On the other hand, β has been reported sensitive to the surface roughness for spherical particles (e.g. Yimsiri and Soga 2000). Fig. 13a shows that β increases from 0.42 (smooth) to 0.49 (rough) for SGB and DGB samples. Otsubo and O'Sullivan (2018) reported experimentally that S_q/D_{50} can be related to β, ranging from 0.38 to 0.54 for spherical glass beads. In this study, SSGB has a non-negligible S_q/D_{50} than Otsubo and O'Sullivan (2018); thus, giving a slightly larger β value of 0.416.

Referring to Fig. 13a, DGB samples exhibit similar trends with SGB samples, whereas AGB and SS samples give different trends in which β is not sensitive to the surface roughness (β= 0.44 to 0.46) (Fig. 13b). RAGB gives even lower β than SAGB, contrary to the observation for SGB and DGB. McDowell and Bolton (2001) reported that β is 0.5 when a conical-shape asperity is in contact with a flat plate; sharp edges of angular grains could cause such a conical-shape contact. It can be concluded that the effect of surface roughness on G_0 is limited for angular materials.

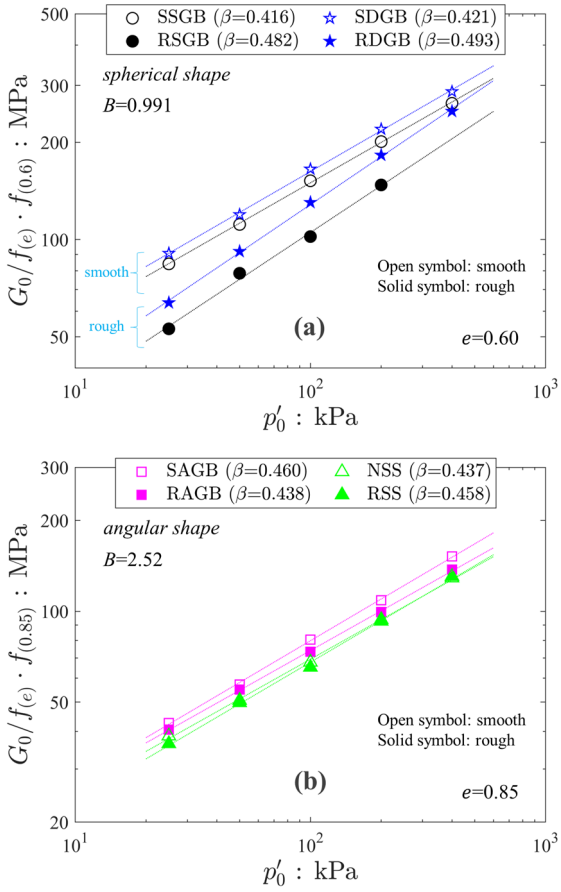

Figure 13. Evolution of G_0 with increasing p_0' (a) *spherical shape* (SGB and DGB) for e=0.6 (b) *angular shape* (AGB and SS) for e=0.85 (β is obtained from Eq. (3)).

6. Conclusions

This contribution explored the influence of grain shape, surface roughness and their combination on the mechanical response of cohesionless granular materials. Based on a series of triaxial compression tests along with shear wave measurements at the initial isotropic stress state, the following conclusions can be drawn:

- Small-strain shear modulus (G_0) of spherical materials is sensitively affected by the surface roughness where G_0 tends to be lower for rougher surface material; however, the stress exponent (β) is higher for materials with rougher surface (Fig. 13a).
- However, the effect of surface roughness is limited for angular materials, i.e. G_0 of angular materials is not sensitive to the difference in surface roughness. β is as high as 0.460 even for the smooth-surface angular glass beads (SAGB) (Fig. 13b).
- The range between e_{max} and e_{min} is different between spherical materials and angular materials. This makes it difficult to discuss the effect of grain shape on G_0 systematically. For the attainable range of e, however, spherical particles (with lower e) tend to give grater V_s and thus G_0 (Fig. 12).
- Peak and residual strengths (i.e. φ_{peak} and φ_{res}) are largely influenced by grain shape, much significant than the effect of surface roughness.
- Increased surface roughness leads to an increase in the φ_{peak} and φ_{res} values. This is more remarkable for angular materials than spherical particles (Figs. 9 and 11). Particularly, this effect is limited for the comparison between SSGB and RSDB (Fig. 5).
- As a side effect, significant fluctuation observed in the stress-strain curves for the smooth-surface spherical particles (SSGB and SDGB) disappear when their surfaces were roughened. This indicates that inter-particle slip can be prevented due to increased surface roughness.

The present contribution has been developed based on Li (2022), focusing on uniformly graded granular materials tested at a relatively low stress level (σ_3'= 50 kPa). Therefore, further research is needed to draw a clearer picture of the combined effect of grain shape and surface roughness on the strain-dependent mechanical response of geomaterials.

Acknowledgements

This work was supported by JSPS KAKENHI Grant Number 22K14322, and JSPS Bilateral Joint Research Projects (JPJSBP120195701) with The Royal Society (IEC\R3\183026).

References

Altuhafi, F. , O'Sullivan, C., Cavarretta, I. 2013. "Analysis of an image-based method to quantify the size and shape of sand particles." J Geotech Geoenviron. 139, no. 8, 1290–1307.
https://doi.org/10.1061/(ASCE)GT.1943-5606.0000855

Altuhafi, F., Coop, M., Georgiannou, V. 2016. "Effect of particle shape on the mechanical behavior of natural sands." J Geotech Geoenviron. 142, no. 12, 04016071.
https://doi.org/10.1061/(ASCE)GT.1943-5606.0001569

Cavarretta, I., Coop, M., O'Sullivan, C. 2010. "The influence of particle characteristics on the behaviour of coarse grained soils." Géotechnique 60, no. 6, 413–423.
https://doi.org/10.1680/geot.2010.60.6.413

Cho, G. C., Dodds, J., Santamarina, J. C. 2006. "Particle shape effects on packing density, stiffness, and strength: natural and crushed sands." J Geotech Geoenviron. 132, no. 5, 591–602.
https://doi.org/10.1061/(ASCE)1090-0241(2006)132:5(591)

Dutta, T., Otsubo, M., Kuwano, R., O'Sullivan, C. 2020. "Evolution of shear wave velocity during triaxial compression." Soils Found. 60, no. 6, 1357–1370.
https://doi.org/10.1016/j.sandf.2020.07.008

Dutta, T., Otsubo, M., Kuwano, R. 2021. "Effect of shearing history on stress wave velocities of sands observed in triaxial compression tests." Soils Found. 61, no. 2, 541–548.
https://doi.org/10.1016/j.sandf.2021.02.002

Hardin, B. O., Richart Jr., F. E. 1963. "Elastic wave velocities in granular soils." J Soil Mech Found Divis. 89, no. 1, 33–66. https://doi.org/10.1061/JSFEAQ.0000493

McDowell, G., Bolton, M., 2001. Micro mechanics of elastic soil. Soils Found. 41, no. 6, 147-152.
https://doi.org/10.3208/sandf.41.6_147

Santamarina, J. C., Cascante, G. 1998. "Effect of surface roughness on wave propagation parameters." Géotechnique 48, no. 1, 129–136. https://doi.org/10.1680/geot.1998.48.1.129

Sharifipour, M., Dano, C. 2006. "Effect of grains roughness on waves velocities in granular packings." In *Proceedings of the First Euro Mediterranean Symposium in Advances on Geomaterials and Structures*, edited by F. Darve, 123–128. Hammamet, Tunisia. https://hal.science/hal-01008097

Otsubo, M., O'Sullivan, C., Sim, W. W., Ibraim, E. 2015. "Quantitative assessment of the influence of surface roughness on soil stiffness." Géotechnique 65, no. 8, 694–700.
https://doi.org/10.1680/geot.14.T.028

Otsubo, M., O'Sullivan, C. 2018. "Experimental and DEM assessment of the stress-dependency of surface roughness effects on shear modulus". Soils Found. 58, no 3, 602–614.
https://doi.org/10.1016/j.sandf.2018.02.020

Li, Y. "Effects of particle morphology on mechanical responses of granular materials", *PhD thesis*, The university of Tokyo, 2022.

Li, Y., Otsubo, M., Kuwano, R., Nadimi, S. 2021. "Quantitative evaluation of surface roughness for granular materials using Gaussian filter method". Powder Technology 388, 251–260. https://doi.org/10.1016/j.powtec.2021.04.068

Yamashita, S., Kawaguchi, T., Nakata, Y., Mikami, T., Fujiwara, T., Shibuya, S. 2009. "Interpretation of international parallel test on the measurement of G_{max} using bender elements." Soils Found. 49, no. 4, 631–650.
https://doi.org/10.3208/sandf.49.631

Yimsiri, S., Soga, K. 2000. "Micromechanics-based stress–strain behaviour of soils at small strains." Géotechnique 50, no. 5, 559–571. https://doi.org/10.1680/geot.2000.50.5.559